PLASMA DIAGNOSTICS OF AN EIT WAVE OBSERVED BY *HINODE*/EIS AND *SDO*/AIA

A. M. VERONIG[1], P. GÖMÖRY[2,3], I. W. KIENREICH[1], N. MUHR[1], B. VRŠNAK[4], M. TEMMER[1], AND H. P. WARREN[5]

[1] Institute of Physics, University of Graz, Universitätsplatz 5, A-8010 Graz, Austria; astrid.veronig@uni-graz.at
[2] Astronomical Institute, Slovak Academy of Sciences, SK-05960 Tatranská Lomnica, Slovakia
[3] Kanzelhöhe Observatory/Institute of Physics, University of Graz, A-9521 Treffen, Austria
[4] Hvar Observatory, Faculty of Geodesy, Kačićeva 26, 1000 Zagreb, Croatia
[5] Space Science Division, Naval Research Laboratory, Washington, DC 20375, USA

ABSTRACT

We present plasma diagnostics of an Extreme-Ultraviolet Imaging Telescope (EIT) wave observed with high cadence in *Hinode*/Extreme-Ultraviolet Imaging Spectrometer (EIS) sit-and-stare spectroscopy and *Solar Dynamics Observatory*/Atmospheric Imaging Assembly imagery obtained during the HOP-180 observing campaign on 2011 February 16. At the propagating EIT wave front, we observe downward plasma flows in the EIS Fe XII, Fe XIII, and Fe XVI spectral lines (log $T \approx 6.1$–6.4) with line-of-sight (LOS) velocities up to 20 km s^{-1}. These redshifts are followed by blueshifts with upward velocities up to -5 km s^{-1} indicating relaxation of the plasma behind the wave front. During the wave evolution, the downward velocity pulse steepens from a few km s^{-1} up to 20 km s^{-1} and subsequently decays, correlated with the relative changes of the line intensities. The expected increase of the plasma densities at the EIT wave front estimated from the observed intensity increase lies within the noise level of our density diagnostics from EIS Fe XIII 202/203 Å line ratios. No significant LOS plasma motions are observed in the He II line, suggesting that the wave pulse was not strong enough to perturb the underlying chromosphere. This is consistent with the finding that no Hα Moreton wave was associated with the event. The EIT wave propagating along the EIS slit reveals a strong deceleration of $a \approx -540$ m s^{-2} and a start velocity of $v_0 \approx 590$ km s^{-1}. These findings are consistent with the passage of a coronal fast-mode MHD wave, pushing the plasma downward and compressing it at the coronal base.

Key words: Sun: corona – Sun: coronal mass ejections (CMEs)

Online-only material: animations

1. INTRODUCTION

Large-scale disturbances propagating through the solar corona have been first imaged by the Extreme-Ultraviolet Imaging Telescope (EIT) onboard the *Solar and Heliospheric Observatory* (*SOHO*) about 15 years ago (Thompson et al. 1998), and colloquially termed "EIT waves." EIT waves have been initially interpreted as the coronal counterparts of Moreton waves, in accordance with the fast-mode coronal MHD wave model developed by Uchida (1968). However, due to statistical differences derived in the propagation velocities of Moreton waves, which are of the order of 1000 km s^{-1}, and EIT waves, which lie mostly in the range 200–400 km s^{-1} (Klassen et al. 2000; Thompson & Myers 2009), this interpretation was questioned and alternative models were developed. Interpretations of EIT waves can be subdivided into wave versus non-wave models. In the non-wave models, EIT waves are explained by the large-scale coronal restructuring due to the erupting coronal mass ejection (CME) causing the observed emission enhancements either due to plasma compression, heating or localized energy release (e.g., Delannée & Aulanier 1999; Chen et al. 2002; Attrill et al. 2007).

Coronal wave studies with the EIT instrument were limited by its 12 minute observing cadence. This situation drastically improved with the launch of the *Solar Terrestrial Relations Observatory* (*STEREO*) in 2006 October, which has led to significant progress in the understanding of these intriguing events. The multi-point observing platforms of the twin *STEREO* satellites with their Extreme-Ultraviolet Imagers (EUVI; Howard et al. 2008) have made it possible to gain insight into the three-dimensional structure and evolution of EUV waves (Patsourakos et al. 2009; Kienreich et al. 2009; Ma et al. 2009;

Temmer et al. 2011), including events where the full three-dimensional coronal wave dome was observed (Veronig et al. 2010). In addition, the high cadence (2.5 minutes), large field of view, and simultaneous observations from two vantage points facilitated the first detailed studies on the wave dynamics and its relation to the associated CME evolution (Patsourakos & Vourlidas 2009; Kienreich et al. 2009; Temmer et al. 2011). Recent *STEREO*/EUVI findings include observations of EIT waves, which undergo a significant deceleration during their propagation, accompanied by a decay of the perturbation amplitude and broadening of the wave front (Veronig et al. 2008, 2010; Long et al. 2011; Muhr et al. 2011). A set of four homologous EIT waves studied in Kienreich et al. (2011) revealed a distinct correlation between the wave speed and the magnetosonic Mach number. These properties are consistent with the behavior of a (weak) fast-mode shock wave. It is important to note that these recent observational improvements also led to significant advancement of MHD simulations of EIT waves (e.g., Cohen et al. 2009; Downs et al. 2011). For recent reviews see Wills-Davey & Attrill (2009), Gallagher & Long (2010), and Zhukov (2011).

Since 2010, the Atmospheric Imaging Assembly (AIA; Lemen et al. 2011) onboard the *Solar Dynamics Observatory* (*SDO*) delivers ultra-high cadence (12 s) multiwavelength imaging of the solar atmosphere. First studies of EIT waves with AIA revealed unexpected fine structures within the diffuse wave front (Liu et al. 2010). Due to the high sensitivity of AIA, more EIT waves with a three-dimensional dome are also reported (e.g., Kozarev et al. 2011). What is still missing, however, is plasma diagnostics of EIT waves, i.e., density, temperature, and plasma flows at the wave front. Such information cannot be obtained with EUV imagers but needs spectroscopic observations.

Harra & Sterling (2003) studied an EIT wave with the Coronal Diagnostics Spectrometer onboard *SOHO*, without detection of significant line-of-sight (LOS) velocities at the wave front (i.e., $v_{LOS} \lesssim 10$ km s^{-1}). Two studies related to EIT waves were performed with the Extreme-Ultraviolet Imaging Spectrometer (EIS; Culhane et al. 2007) on board *Hinode* (Asai et al. 2008; Chen et al. 2010) but the EIS observing mode was not suitable to study the plasma characteristics and motions at the EIT wave front. In this Letter, we present EIS plasma diagnostics of the EIT wave of 2011 February 16 based on a unique data set obtained during our *Hinode* Observing Plan HOP-180,[6] where we combined high-cadence sit-and-stare EIS spectroscopy with high-cadence imaging by AIA. EIS LOS plasma motions and line widths for the event under study have been presented in Harra et al. (2011), whereas here we concentrate on the relation between the different plasma parameters (including plasma densities and flows) at the wave front and their evolution.

2. DATA

Hinode/EIS is a two-channel, normal-incidence EUV spectrometer observing in the wavelength ranges 170–210 Å and 250–290 Å (Culhane et al. 2007). The high EIS spectral resolution allows Doppler velocity measurements of plasma flows better than ± 5 km s^{-1}. In order to study the plasma characteristics at propagating EIT wave fronts, we defined a dynamic EIS observing programme, which combines high-cadence *Hinode*/EIS spectroscopy and *SDO*/AIA imaging. This programme was accepted as HOP-180 and realized during 2011 February 11–17. In HOP-180 we performed high-cadence EIS spectroscopic sit-and-stare observations (45 s exposure + 4 s readout time), placing the spectrometer slit (width: 1″ and length: 512″) on the border of an active region, in order to follow the evolution of EIT waves along the EIS slit with a spatial sampling of 1″ pixel^{-1}. We selected 11 EIS spectral lines over the temperature range log $T = 4.7$ to 6.7, including line pairs from the same ion for density diagnostics. On 2011 February 16 EIS observed an EIT wave propagating along its slit (see Figure 1), on which we concentrate in this study.

Basic EIS photometric correction and correction of the orbital motion of the satellite were applied using the eis_prep.pro and eis_wave_corr.pro routines, before the spectral profiles were fitted by a single Gaussian function with a linear background to obtain the spectral intensities, integrated intensities, background intensities, Doppler shifts, and spectral widths. The zero reference of the Doppler shifts were calculated as the average value of the Doppler shifts from quiet-Sun regions. From the Fe XIII 202/203 Å line pair we derived the coronal electron densities from the theoretical variation of the line ratio with density using the CHIANTI database version 6.0.1. (Dere et al. 1997, 2009). Once the theoretical ratio was known, the final density maps were calculated using the EIS routine eisdensity.pro.

The EIT wave under study was also observed by *SDO*/AIA, which carries four (E)UV telescopes providing full-Sun images in 10 different wavelengths at a cadence as high as 12 s and spatial resolution of 1″.5 (with 0″.6 pixels). In this study, we use in particular the AIA 211 Å (log $T = 6.3$) and 193 Å (log $T = 6.1$) filters, in which the EIT wave signal was highest.

3. RESULTS

Figure 1 shows a sequence of *SDO*/AIA 211 Å direct and running ratio images together with the location of the

Hinode/EIS spectrometer slit. The EIT wave was launched in association with the M2 flare/CME event from AR 11158, and revealed a global propagation mainly toward the northern hemisphere. In particular, a distinct segment of the wave propagated along the EIS slit northward toward AR 11159 (see also Movies 1 and 2 in the online journal).

Figure 2 shows stack plots of LOS velocities and intensities derived from the EIS Fe XIII 202 Å spectra. During about 14:23 to 14:38 UT we observe a narrow lane of redshifts indicating LOS velocities up to 20 km s^{-1} (Figure 2(a)) correlated with a bright lane in the Fe XIII intensities (Figures 2(b) and (c)) with enhancements up to about 25% above the pre-event level. Co-aligned *SDO*/AIA images confirm that these signatures are due to the EIT wave front passing the EIS slit (see movie 1). The peaks of the EIS intensity enhancements at the EIT wave front tend to occur delayed by one time step ($\approx$49 s) with regard to the EIS LOS velocity pulses, suggesting that the intensity change is a reaction to the downward push of the coronal plasma below the wave front. The brightest feature around 14:22 UT at $y \approx -255''$ is due to the associated M2 flare (Harra et al. 2011).

The EIT wave front visible as a narrow lane of redshifts in the EIS LOS velocities is followed by blueshifted pattern indicating relaxation of the plasma behind the wave front, with upward velocities $|v_{LOS}| < 5$ km s^{-1} (Figure 2(a)). Behind this lane of blueshifts there is a broader lane of redshifts indicating another propagating feature with downward-directed plasma motions and concurrent intensity enhancements. Since these LOS velocities are of the same order than that of the first lane of redshifts, i.e., up to about 20 km s^{-1}, they cannot be due to another swing of the primary EIT wave but are rather due to a second disturbance moving behind. In addition, there is a distinct dark lane observed in the EIS intensitygrams (Figure 2(b)), indicating propagation along the EIS slit with velocities of $\approx$120 $\pm$ 10 km s^{-1}, but with no reflection in the LOS velocities (Figures 2(a) and (c)). *SDO*/AIA images reveal that this signal is due to an ejecta moving northward along the slit (see online movie 1).

Figure 2(d) shows stack plots of plasma densities derived from the EIS Fe XIII 202/203 Å line pair. At the early phase of the EIT wave evolution, there is evidence of a lane of enhanced density between about $y = -200''$ and $-100''$, roughly cospatial with the propagating EIT wave. However, careful comparison reveals that the enhanced densities are located about two to three time steps ($\sim$100–150 s) behind the wave front. At the positions of the density enhancements we observe decreased intensities and plasma upflows up to about -50 km s^{-1} (cf. Figures 2(a) and (b)). Thus, we interpret this enhanced density feature as being related to the eruption *behind* the EIT wave and not due to plasma compression at the wave front itself. In the range $y = +120''$ to $+180''$ there is some indication of a density depletion evolving with the EIT wave.

The distinct LOS velocity signal at the propagating EIT wave front is also well observed in the EIS Fe XII 195 Å spectral line (log $T = 6.11$) but the LOS velocities are on average 5 km s^{-1} smaller than in the Fe XIII 202 Å line. In Fe XVI 262 Å (log $T = 6.4$), a weak signature of the EIT wave can be observed. There is no significant signal of the EIT wave in the He II 256 Å line (log $T = 4.7$), indicating that the upper chromosphere was basically unaffected by the passing EIT wave front. This is consistent with the high-cadence Hα observations by HASTA (Hα Solar Telescope for Argentinia), which show no signs of a Moreton wave. We also note that in the hotter spectral lines we observed no clear signal related to

---
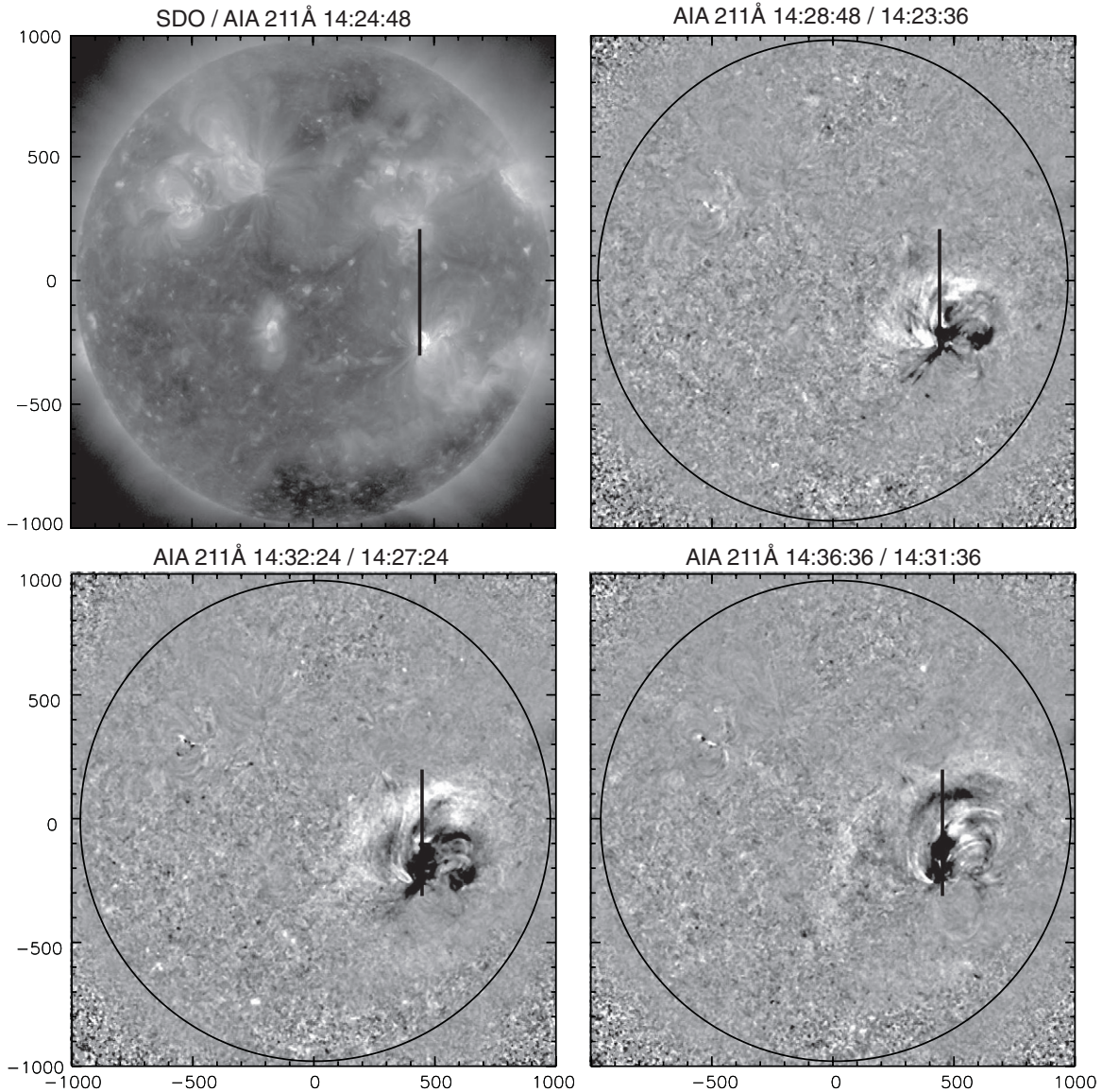
Figure 1. Sequence of *SDO*/AIA 211 Å direct (top left) and running ratio images. The vertical line indicates the position of the *Hinode*/EIS spectrometer slit. The accompanying movie 1 shows the EIT wave evolution in *SDO*/AIA 211 Å direct and running ratio images. Movie 2 shows the same in the *SDO*/AIA 193 Å filter.
(Animations of this figure are available in the online journal.)

the EIT wave except some signature in the Ca XVII 192 Å line (log $T = 6.7$), which we attribute to a blend by Fe XI. Figure 3 shows cuts through the Fe XII and Fe XIII velocity stack plots, revealing the propagating LOS velocity pulse. From these plots we derive the time, location, and amplitude of the LOS velocity peaks used in the following to study the wave kinematics and the plasma characteristics with EIS.

In addition, we calculated the EIT wave kinematics also from *SDO*/AIA 211 Å running ratio images. The center derived from circular fits to the earliest wave fronts ($x = 462'' \pm 29''$ and $y = -267'' \pm 21''$) lies almost on the EIS slit, and we thus calculated both the AIA and EIS wave kinematics as the distance of the wave fronts along the spherical solar surface (see Veronig et al. 2006) to the pixel located at the EIS slit at $x = 440''$ and $y = -267''$. The resulting *SDO*/AIA and *Hinode*/EIS kinematics are shown in Figure 4(a), evidencing a strong deceleration of the EIT wave. The quadratic fit to the AIA measurements gives a start velocity $v_0 = 585 \pm 56$ km s^{-1} and deceleration $a = -675 \pm 160$ m s^{-2}; the mean velocity is

$\bar{v} = 336 \pm 15$ km s^{-1}. These values are consistent with the results we obtain from calculating the EIT wave kinematics from the positions of the peaks of the *Hinode*/EIS Fe XIII LOS velocities, where we find $v_0 = 587 \pm 50$ km s^{-1}, $a = -539 \pm 48$ m s^{-2}, and $\bar{v} = 371 \pm 12$ km s^{-1}.

Figure 4(b) shows the evolution of the peak of the EIS Fe XIII LOS velocity pulse at the wave front, revealing an increase of the pulse during 14:24 UT up to 14:28 UT from ~3–5 to 15–20 km s^{-1}, and a subsequent decay during the remaining wave evolution. We also note that the EIT wave observed in AIA imagery revealed different characteristics in different propagation directions. The fastest propagation occurred into the NW quadrant, where we find a start velocity $v_0 = 756 \pm 56$ km s^{-1}, deceleration $a = -489 \pm 160$ m s^{-2}, and mean velocity $\bar{v} = 576 \pm 15$ km s^{-1}.

If the EIT wave under study is due to a coronal fast-mode wave pushing the plasma downward and compressing it, we expect a correlation between the amplitude of the velocity pulse and the change in plasma density and intensity at the wave front. To test
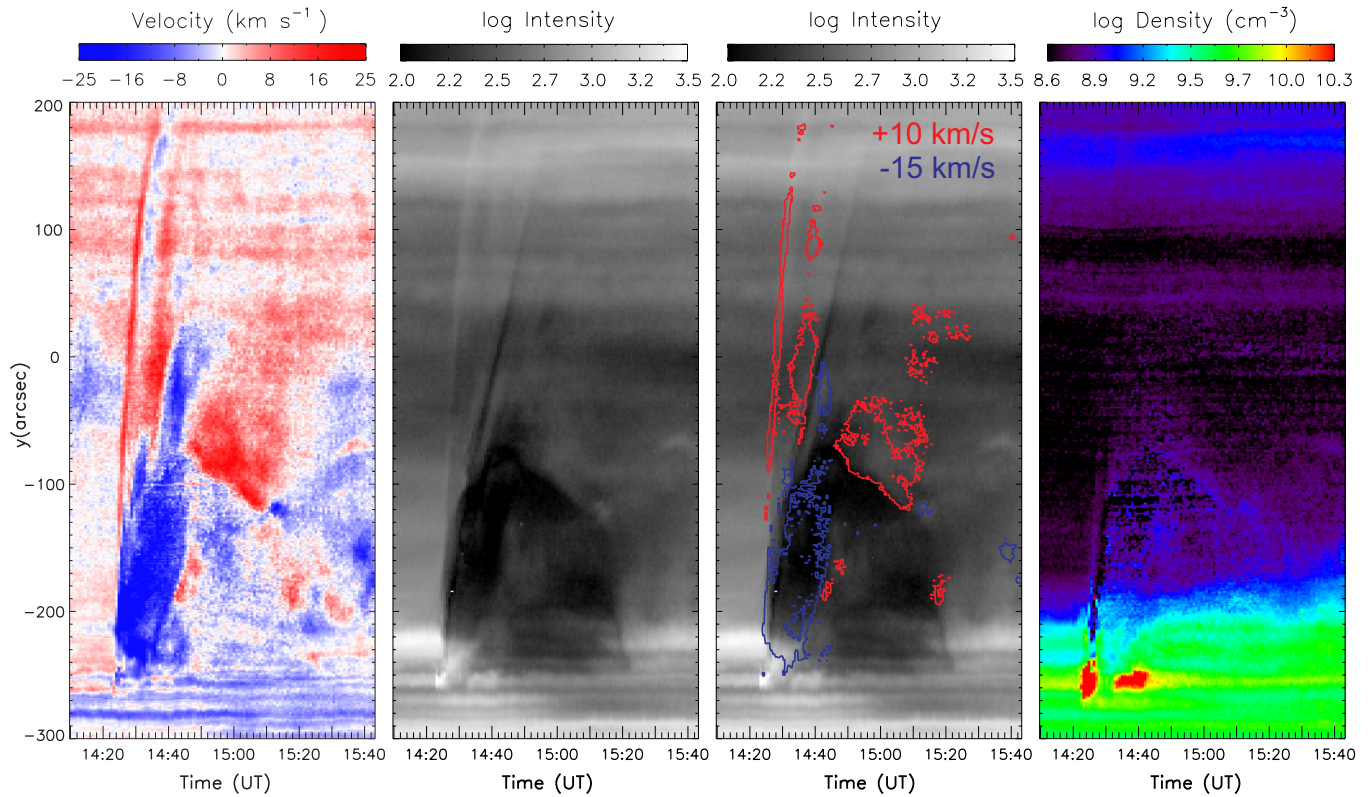
Figure 2. Stack plots showing the Fe XIII 202 Å evolution along the EIS slit during the time range 14:10 to 15:42 UT: (a) velocities, (b) intensities, (c) intensities together with velocity contours at −15 km s^{-1} (blue) and +10 km s^{-1} (red), and (d) densities derived from the Fe XIII 202/203 Å line pair.
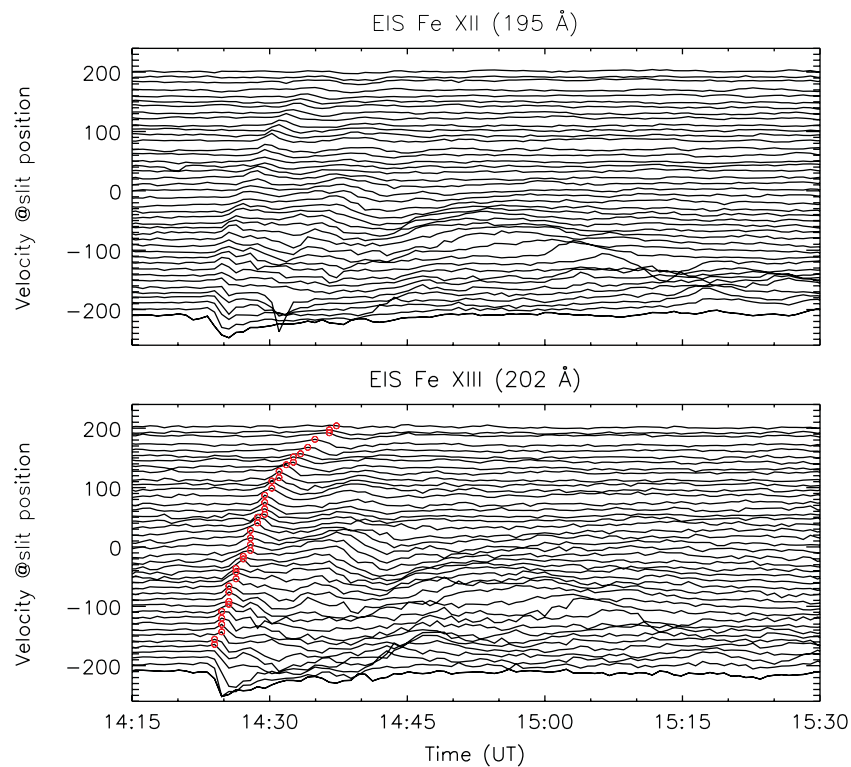
Figure 3. Velocity profiles derived from the EIS Fe XII (top) and Fe XIII (bottom) spectrograms (only each 10th profile available is plotted). Each profile starts at the y-position along the slit. The circles plotted on top of the Fe XIII profiles indicate the position of the peak LOS velocity at the wave front. These positions/values are used for the EIS wave kinematics (Figure 4(a)) and LOS velocity evolution (Figure 4(b)) as well as for the correlation plots in Figure 5.
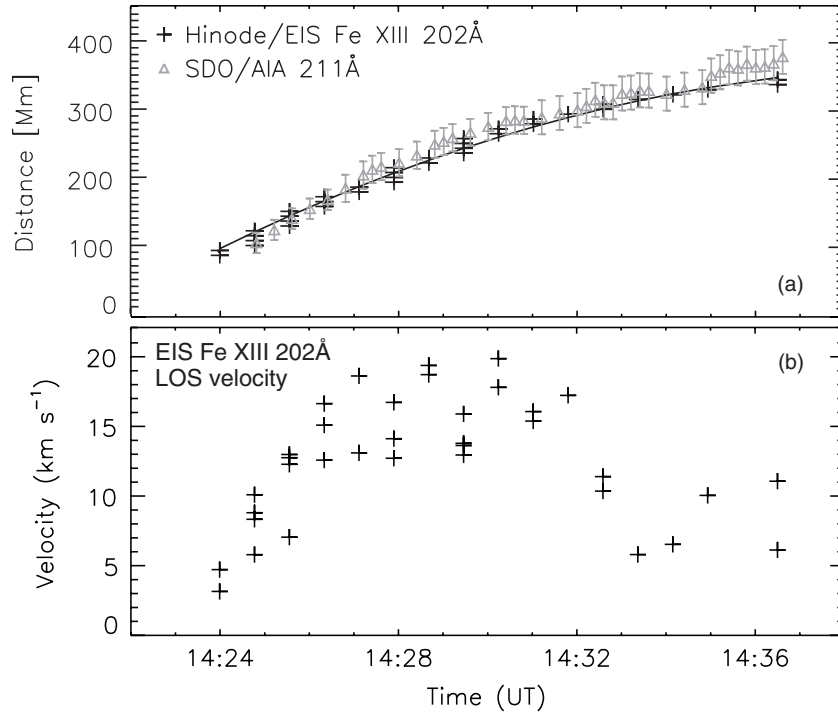
Figure 4. (a) Kinematics of the EIT wave derived from the EIS Fe XIII LOS velocity peaks (crosses) and from the wave fronts identified in *SDO*/AIA 211 Å images (triangle with error bars). (b) Evolution of the EIS Fe XIII LOS velocity peaks derived at the EIT wave front (cf. Figure 3, bottom).
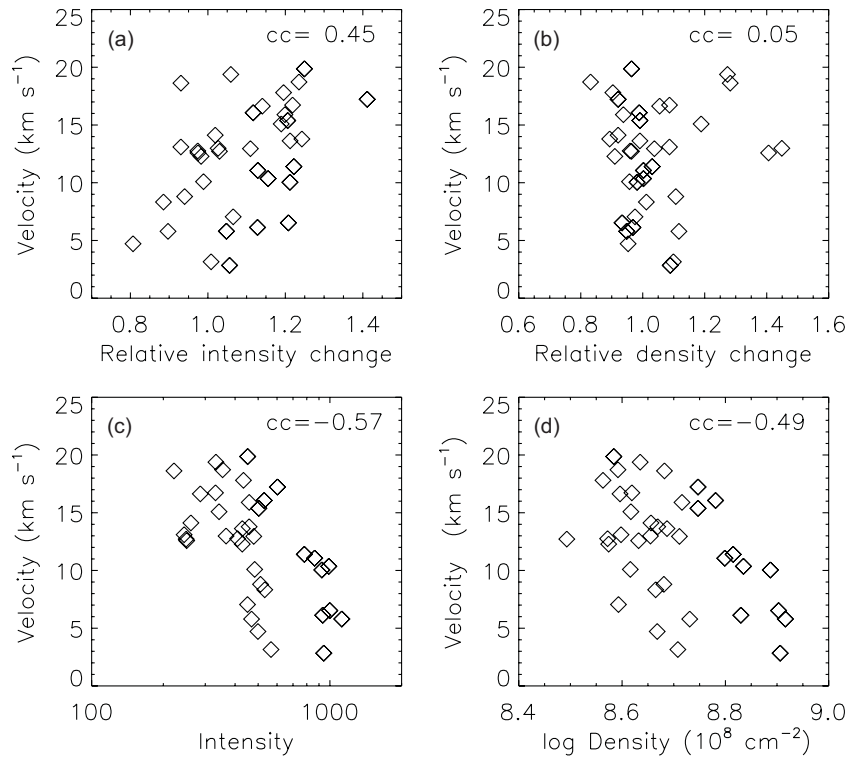
Figure 5. Correlation plots of the EIS Fe XIII LOS velocity against the relative changes (top) and absolute values (bottom) of the intensity and density at the EIT wave front.

this hypothesis, we calculate the relative changes of these plasma parameters with respect to the pre-event conditions by dividing each EIS density and intensity value by the corresponding pixel prior to the EIT wave. The correlation plots for the EIS Fe XIII parameters are shown in the top panels of Figure 5, where we shifted the extracted EIS intensity values by one time step (49 s)

with respect to the LOS velocities to account for their delayed response. Indeed, for the relationship LOS velocity against intensity changes we obtain a positive correlation (cc = 0.45) indicating that large downward velocities due to the passing EIT wave front are correlated with enhanced intensities, which are usually attributed to plasma compression (e.g., Klassen

et al. 2000). However, no such correlation is found between the LOS velocity and the relative changes in density. This lack of correlation may be due to temperature enhancements as well as plasma compression contributing to the intensity changes or due to uncertainties involved in the density derivation. The maximum changes of intensities we observe at the EIT wave front are 25% (except for one data point; see Figure 5(a)). Assuming that the intensity enhancements at the wave front are solely due to enhanced plasma densities (and not due to changes in temperature), the maximum density increase expected is about 10% ($I \propto n^2$ for $T =$ const). This indeed lies within the noise level of our density estimates (cf. Figure 2(d)).

The bottom panels in Figure 5 show scatter plots of the LOS velocities against the absolute values of the EIS Fe XIII intensities and densities at the EIT wave front, revealing a distinct anti-correlation (intensities: cc $= -0.57$; densities: cc $= -0.49$). The observed intensities and densities actually combine the LOS-integrated optically thin contributions of both the coronal "background" plasma as well as the changes caused by the EIT wave. The anti-correlation obtained for the absolute values may be related to the different states of "background" corona through which the wave propagates. Assuming conservation of the wave's energy flux $\rho v^2/2$, the LOS velocity caused by the passing wave front will be smaller when propagating through a plasma of high magnetic and gas pressure such as in an active region (appearing as horizontal stripe of high EUV intensity and enhanced density in Figures 2(b) and (d)) because the plasma is more inert than in a quiet region where the magnetic and gas pressure are small. This is a simplified picture, since the wave properties themselves are also expected to change during the propagation, in terms of intensification and decay of the wave pulse, but it can qualitatively explain the observed anti-correlations.

4. DISCUSSION AND CONCLUSIONS

High-cadence EIS sit-and-stare spectroscopy combined with high-cadence AIA imaging allowed us to study the plasma characteristics and evolution of a fast EIT wave that occurred on 2011 February 16. The fastest propagation was observed toward the NW quadrant from the source AR 11158 with a mean velocity of 580 km s^{-1}, whereas the propagation along the EIS slit toward AR 11158 in the northern direction revealed a mean velocity of about 370 km s^{-1}. We observe downward plasma flows in coronal spectral lines formed at temperatures in the range 1.2–2.5 MK co-aligned with the intensity enhancements at the propagating EIT wave front. On average the peaks of the EIS intensity enhancements at the EIT wave front occur delayed by ≈ 1 minute with respect to the redshifted velocity pulses, suggesting that the intensity change is a reaction to the downward push of the coronal plasma below the wave front. The peak LOS velocities of the downward plasma motions reach values up to 20 km s^{-1} followed by upward velocities up to -5 km s^{-1} indicative of relaxation of the plasma behind the passing EIT wave front.

The downward plasma motions at the wave front reveal initial intensification and subsequent decay, correlated with the relative changes of the EIS spectral line intensities, in line with the expectation for a fast-mode MHD wave. However, no correlation is found between the relative density changes and the LOS velocities. This lack of correlation is assumed to be due to the uncertainties of the density estimates which are of the same order as the relative density enhancements expected from the observed wave front intensities (which are $\lesssim 25\%$). To settle this issue,

spectroscopic observations of EIT waves of larger amplitudes are needed. For comparison, in the EIT waves studied in Muhr et al. (2011), relative intensity changes up to 70% have been reported. In addition to the decay of the LOS velocity pulse we also observe a significant deceleration of the EIT wave during its propagation ($a \approx -540$ m s^{-2}).

Our findings are consistent with the interpretation that the EIT wave under study is a coronal fast-mode MHD wave, pushing the plasma downward and compressing it at the coronal base though we note that definitive density diagnostics is still missing. In contrast, non-wave models attributing the EIT wave to magnetic restructuring during the CME lift-off or to forced magnetic reconnection ahead of the CME front do not predict a downward push of the lower corona. In the He II line, no significant plasma motions at the EIT wave front are detected, consistent with the fact that no Hα Moreton wave was associated. This finding implies that in the EIT wave under study the observed coronal wave pulse with LOS velocities $\lesssim 20$ km s^{-1} was not strong enough to perturb the underlying "dense" chromosphere.

REFERENCES

Asai, A., Hara, H., Watanabe, T., et al. 2008, ApJ, 685, 622
Attrill, G. D. R., Harra, L. K., van Driel-Gesztelyi, L., & Démoulin, P. 2007, ApJ, 656, L101
Chen, F., Ding, M. D., & Chen, P. F. 2010, ApJ, 720, 1254
Chen, P. F., Wu, S. T., Shibata, K., & Fang, C. 2002, ApJ, 572, L99
Cohen, O., Attrill, G. D. R., Manchester, W. B., IV, & Wills-Davey, M. J. 2009, ApJ, 705, 587
Culhane, J. L., Harra, L. K., James, A. M., et al. 2007, Sol. Phys., 243, 19
Delannée, C., & Aulanier, G. 1999, Sol. Phys., 190, 107
Dere, K. P., Landi, E., Mason, H. E., Monsignori Fossi, B. C., & Young, P. R. 1997, A&AS, 125, 149
Dere, K. P., Landi, E., Young, P. R., et al. 2009, A&A, 498, 915
Downs, C., Roussev, I. I., van der Holst, B., et al. 2011, ApJ, 728, 2
Gallagher, P. T., & Long, D. M. 2010, Space Sci. Rev., 158, 365
Harra, L. K., & Sterling, A. C. 2003, ApJ, 587, 429
Harra, L. K., Sterling, A. C., Gömöry, P., & Veronig, A. 2011, ApJ, 737, L4
Howard, R. A., Moses, J. D., Vourlidas, A., et al. 2008, Space Sci. Rev., 136, 67
Kienreich, I. W., Temmer, M., & Veronig, A. M. 2009, ApJ, 703, L118
Kienreich, I. W., Veronig, A. M., Muhr, N., et al. 2011, ApJ, 727, L43
Klassen, A., Aurass, H., Mann, G., & Thompson, B. J. 2000, A&AS, 141, 357
Kozarev, K. A., Korreck, K. E., Lobzin, V. V., Weber, M. A., & Schwadron, N. A. 2011, ApJ, 733, L25
Lemen, J. R., et al. 2011, Sol. Phys., in press
Liu, W., Nitta, N. V., Schrijver, C. J., Title, A. M., & Tarbell, T. D. 2010, ApJ, 723, L53
Long, D. M., Gallagher, P. T., McAteer, R. T. J., & Bloomfield, D. S. 2011, A&A, 531, A42
Ma, S., Wills-Davey, M. J., Lin, J., et al. 2009, ApJ, 707, 503
Muhr, N., Veronig, A. M., Temmer, M., Kienreich, I., & Vršnak, B. 2011, ApJ, 739, 89

Patsourakos, S., & Vourlidas, A. 2009, ApJ, 700, L182
Patsourakos, S., Vourlidas, A., Wang, Y. M., Stenborg, G., & Thernisien, A. 2009, Sol. Phys., 259, 49
Temmer, M., Veronig, A. M., Gopalswamy, N., & Yashiro, S. 2011, Sol. Phys., in press
Thompson, B. J., & Myers, D. C. 2009, ApJS, 183, 225
Thompson, B. J., Plunkett, S. P., Gurman, J. B., et al. 1998, Geophys. Res. Lett., 25, 2465
Uchida, Y. 1968, Sol. Phys., 4, 30
Veronig, A. M., Muhr, N., Kienreich, I. W., Temmer, M., & Vršnak, B. 2010, ApJ, 716, L57
Veronig, A. M., Temmer, M., & Vršnak, B. 2008, ApJ, 681, L113
Veronig, A. M., Temmer, M., Vršnak, B., & Thalmann, J. K. 2006, ApJ, 647, 1466
Wills-Davey, M. J., & Attrill, G. D. R. 2009, Space Sci. Rev., 149, 325
Zhukov, A. N. 2011, J. Atmos. Sol.-Terr. Phys., 73, 1096